AGU PUBLICATIONS

JGR

Journal of Geophysical Research: Oceans

RESEARCH ARTICLE

10.1002/2015JC010770

Key Points:
- A theory is developed to explicitly model sea ice floe size distribution (FSD)
- The FSD theory is coupled with an ice thickness distribution theory
- Simulated FSD obeys a power law as observed in satellite data

Correspondence to:
J. Zhang,
zhang@apl.washington.edu

Citation:
Zhang, J., A. Schweiger, M. Steele, and H. Stern (2015), Sea ice floe size distribution in the marginal ice zone: Theory and numerical experiments, *J. Geophys. Res. Oceans*, *120*, 3484–3498, doi:10.1002/2015JC010770.

Received 6 FEB 2015
Accepted 20 APR 2015
Accepted article online 24 APR 2015
Published online 12 MAY 2015

Sea ice floe size distribution in the marginal ice zone: Theory and numerical experiments

Jinlun Zhang[1], Axel Schweiger[1], Michael Steele[1], and Harry Stern[1]

[1]Applied Physics Laboratory, Polar Science Center, University of Washington, Seattle, Washington, USA

Abstract To better describe the state of sea ice in the marginal ice zone (MIZ) with floes of varying thicknesses and sizes, both an ice thickness distribution (ITD) and a floe size distribution (FSD) are needed. In this work, we have developed a FSD theory that is coupled to the ITD theory of Thorndike et al. (1975) in order to explicitly simulate the evolution of FSD and ITD jointly. The FSD theory includes a FSD function and a FSD conservation equation in parallel with the ITD equation. The FSD equation takes into account changes in FSD due to ice advection, thermodynamic growth, and lateral melting. It also includes changes in FSD because of mechanical redistribution of floe size due to ice ridging and, particularly, ice fragmentation induced by stochastic ocean surface waves. The floe size redistribution due to ice fragmentation is based on the assumption that wave-induced breakup is a random process such that when an ice floe is broken, floes of any smaller sizes have an equal opportunity to form, without being either favored or excluded. To focus only on the properties of mechanical floe size redistribution, the FSD theory is implemented in a simplified ITD and FSD sea ice model for idealized numerical experiments. Model results show that the simulated cumulative floe number distribution (CFND) follows a power law as observed by satellites and airborne surveys. The simulated values of the exponent of the power law, with varying levels of ice breakups, are also in the range of the observations. It is found that floe size redistribution and the resulting FSD and mean floe size do not depend on how floe size categories are partitioned over a given floe size range. The ability to explicitly simulate multicategory FSD and ITD together may help to incorporate additional model physics, such as FSD-dependent ice mechanics, surface exchange of heat, mass, and momentum, and wave-ice interactions.

1. Introduction

Significant decline of Arctic sea ice has been observed in recent years [e.g., *Meier et al.*, 2014]. The decline was particularly steep during summers 2007–2013, when the Arctic sea ice extent decreased to the lowest levels observed in the satellite era [e.g., *Comiso*, 2012]. Severe summer melt back leads to increasing areas of warming open water and marginal ice zone (MIZ) [e.g., *Steele et al.*, 2010; *Strong and Rigor*, 2013]. The MIZ is generally defined as a transition region from open water to pack ice with low concentration, low thickness, and diffuse sea ice floes of varying shapes and sizes [*Rothrock and Thorndike*, 1984; *Wadhams*, 1986]. This is in contrast to the thicker, more compact sea ice field in the central Arctic that appears more as a continuum with pressure ridges and leads/cracks interspersed [e.g., *Wadhams*, 1981; *Hibler*, 2001]. The state of sea ice in a given area, whether in MIZ or the central Arctic, may be described by an ice thickness distribution (ITD) that gives the fractions of open water/leads and various ice thicknesses in that area [*Thorndike et al.*, 1975; *Hibler*, 1980]. The *Thorndike et al.* [1975] ITD theory has been increasingly incorporated in operational forecast and climate models. However, the ITD does not give a complete picture of the MIZ that consists of ice floes with diameters ranging from meters to kilometers. Such a character may be represented by a floe size distribution (FSD) [*Rothrock and Thorndike*, 1984; *Holt and Martin*, 2001; *Herman*, 2010]. Thus both FSD and ITD are needed to better capture the state of sea ice in the MIZ.

The evolution of FSD in the MIZ is controlled by dynamic and thermodynamic processes. These processes differ significantly from those in the ice pack interior, including changes in ice-albedo feedbacks, modifications in surface exchanges of heat, mass, and momentum, alterations in sea ice mechanical behavior, and variations in oceanic heat flux. While winds and currents may cause ice to deform and

crack, ice in the MIZ is particularly vulnerable to ocean surface waves and swell that form in the open water, resulting from strong winds and often storms, and propagate into the ice field [*Squire et al*., 1995; *Squire*, 2007; *Kohout et al*., 2014]. While the ice tends to attenuate the incoming waves because of wave-ice interactions [*Wadhams et al*., 1988; *Meylan et al*., 2014], the waves tend to bend ice repeatedly, and the ice breaks if the bending-induced stresses exceed its flexural strength or if the repeated bending leads to fatigue failure [e.g., *Langhorne et al*., 1998]. Once an ice floe is broken, it becomes floes of smaller sizes, a process of floe size redistribution via mechanical forcing. Thus wave conditions (wave energy, frequency, direction, etc.) and wave-ice interactions play a prominent role in determining the magnitude of ice breakups and mechanical floe size redistribution and therefore FSD in the MIZ.

The FSD is often described as the area or the number of floes over a range of floe sizes. A measure of the size of a floe is the caliper diameter defined as the average over all angles of the distance between two parallel lines (or calipers) that are set against the floe's sidewalls [*Rothrock and Thorndike*, 1984; also see *Steele*, 1992]. Analyses of satellite images and aerial photographs reveal that FSD generally obeys a power law [*Rothrock and Thorndike*, 1984; *Holt and Martin*, 2001; *Toyota et al*., 2006; *Steer et al*., 2008]. These analyses indicate that the number of floes per unit area with caliper diameters not smaller than l, or the (reverse) cumulative floe number distribution (CFND), can be described by a power law function $N(l) \propto l^{-\alpha}$, where $N(l)$ is the CFND and l is the caliper diameter of a floe. The significance of the power law is the scale invariance: there is no natural length scale, and the features look the same under arbitrary magnification. The CFND is characterized by a single exponent α over all floe sizes. The power law function is a straight line in a log-log plot and $-\alpha$ is the slope of the line. The α values are often found to vary from 1.15 to 2.90 [*Rothrock and Thorndike*, 1984; *Holt and Martin*, 2001; *Toyota et al*., 2006; *Steer et al*., 2008; *Perovich and Jones*, 2014], indicating varying magnitudes of ice breakups depending on wind and wave forcing and ice conditions.

The FSD is considered important to various aspects of MIZ processes. For example, FSD influences mechanical properties of the ice and thus its response to winds and ocean waves and currents [e.g., *Shen et al*., 1987; *Feltham*, 2005], which is likely to modify the air-sea momentum transfer. FSD also has a significant role in lateral melting [e.g., *Steele*, 1992]. Because lateral melting occurs at the perimeter of ice floes, small floes disappear more quickly than large floes, since they have more perimeter per unit area, and this modifies the FSD. Lateral melting also expands the area of open water more rapidly than top or bottom melting. More rapid shrinking of ice floes with relatively high surface albedo and expansion of open water with low surface albedo would cause positive ice-albedo feedback that tends to enhance the surface absorption of solar energy, elevate ocean surface warming, and accelerate ice retreat [*Perovich et al*., 2007, 2008; *Zhang et al*., 2008]. The lateral melting rate depends on the total perimeter of ice floes occupying a given area. For power law FSDs, the value of the total perimeter is very sensitive to the exponent of the FSD [*Toyota et al*., 2006]. That is, the lateral melting rate is very sensitive to FSD.

Significant progress has been made in modeling FSD-related MIZ processes [e.g., *Dumont et al*., 2011; *Williams et al*., 2013a, b]. Nevertheless, much remains to be done theoretically and numerically to represent the MIZ processes in general and to explicitly simulate the evolution of FSD in particular. Modeling the evolution of FSD as a prognostic state variable is hindered by the fact that many of the MIZ processes are not well understood, such as wave-ice interactions, wave-induced breakup of pack ice, and mechanical floe size redistribution. The knowledge gaps in MIZ processes make it difficult to incorporate FSD into a model. This is why many of the MIZ-relevant processes are not included in operational forecast or climate models. For example, to our knowledge, no large-scale sea ice models are able to explicitly simulate the evolution of FSD in the MIZ, not to mention simulating FSD and ITD jointly. The complexity and difficulty of capturing the MIZ dynamic and thermodynamic processes and the combined evolution of FSD and ITD pose a significant challenge to the operational forecasting and climate modeling community.

This study is meant to be a step forward toward incorporating FSD into large-scale dynamic thermodynamic sea ice models that are based on the ITD theory of *Thorndike et al*. [1975]. We introduce a FSD theory that is closely coupled with the ITD theory. The FSD theory includes a FSD function and an associated FSD conservation equation to describe the sea ice system in the MIZ, in conjunction with the ITD function and the associated ITD conservation equation. An important component of the FSD theory is the description of mechanical redistribution of floe size due to wave-induced ice fragmentation (breakup). To assess the behavior of the FSD theory and, particularly, the properties of its mechanical floe size redistribution, the

FSD conservation equation is incorporated into a simplified zero-dimensional ITD and FSD sea ice model, which is integrated for a series of numerical experiments. The FSD theory is presented in section 3, after a brief description of the ITD equation in section 2. The design of the idealized numerical experiments is presented in section 4. In section 5, results from these experiments are examined. Conclusions are given in section 6.

2. Brief Review of the ITD Equation

Before introducing FSD theory, it is useful to briefly review the *Thorndike et al*. [1975] ITD theory. In the ITD theory, the ice mass conservation is described by an ITD equation

$$\frac{\partial g_h}{\partial t} = -\nabla \cdot (\mathbf{u} g_h) - \frac{\partial (f_h g_h)}{\partial h} + \Psi, \tag{1}$$

where g_h is the ice thickness distribution function, t is time, $\mathbf{u}$ is ice velocity vector, f_h is ice growth rate, h is ice thickness, and Ψ is a mechanical thickness redistribution function for ridging. The thickness redistribution function consists of two terms $\Psi = \Psi_0 + \Psi_r$, which describe the mechanical changes in ITD due to open water creation (Ψ_0) and ridging (Ψ_r) that transfers thin ice to thick ice categories [*Hibler*, 1980]. These two terms can be written as [*Thorndike et al*., 1975; *Hibler*, 1980]

$$\Psi_0 = (P^{*-1} \sigma_{ij} \dot{\varepsilon}_{ij} + \dot{\varepsilon}_{kk}) \delta(h) \tag{2}$$

and

$$\Psi_r = \frac{P^{*-1} \sigma_{ij} \dot{\varepsilon}_{ij} [-P(h) g_h(h) + \int_0^\infty \gamma(h', h) P(h') g_h(h') dh']}{\int_0^\infty [P(h) g_h(h) - \int_0^\infty \gamma(h', h) P(h') g_h(h') dh'] dh}, \tag{3}$$

where P^* is the ice strength, σ_{ij} is the ice stress tensor, $\dot{\varepsilon}_{ij}$ is the ice strain rate tensor, δ is the Dirac delta function, P is the redistribution probability function specifying which categories of ice participate in ridging, and $\gamma(h', h)$ is a redistributor of the ITD. The redistribution probability function P is formulated such that [*Thorndike et al*., 1975; *Hibler*, 1980]

$$P(h) = \max [(1 - \int_0^h g_h(h') dh' / c_r), 0], \tag{4}$$

where constant c_r is a participation factor that specifies an area fraction of thin ice to participate in ridging.

As shown in (1), the *Thorndike et al*. ITD theory assumes that changes in the ITD are due to ice advection, thermodynamic growth or decay, lead opening (open water creation), and ridging. The ITD theory is augmented by an ice enthalpy distribution theory to conserve thermal energy of ice [*Zhang and Rothrock*, 2001, 2003]. The thickness and enthalpy distribution (TED) sea ice model can be used to integrate over multiple subgrid categories each for ice thickness and ice enthalpy [e.g., *Zhang et al*., 2012]. The TED sea ice model integration also includes multiple categories of snow depth following *Flato and Hibler* [1995; also see *Zhang and Rothrock*, 2003].

3. Theory of FSD

To derive a FSD equation, we first define FSD as the fraction of area covered by ice floes with a caliper diameter between l and $l + dl$, such that

$$\int_l^{l+dl} g_l(l) dl = \frac{1}{R} r_l(l, l+dl), \tag{5}$$

where g_l is the FSD function, l is the caliper diameter, R is the total area of some fixed region Ω about the point of interest, and r_l is the area in Ω covered by open water and ice floes with caliper diameters between l and $l + dl$. Integrating (5) over all floe sizes gives

$$\int_0^\infty g_l(l)dl = 1. \tag{6}$$

We consider that FSD, like ITD, is subject to changes caused by ice advection, thermodynamic growth or decay, lead opening, and ridging. With a focus on the MIZ, we further consider that FSD is subject to changes due to fragmentation induced by waves and swell in the MIZ. Thus, we can derive a mathematical equation to describe the FSD evolution in the MIZ such that

$$\frac{\partial g_l}{\partial t} = -\nabla \cdot (\mathbf{u} g_l) - \frac{\partial (f_l g_l)}{\partial l} + \Phi, \tag{7}$$

where f_l is the rate of change in floe size (caliper diameter l) and Φ is the mechanical floe size redistribution function. The second term in (7) describes the change in FSD due to ice advection. The third term describes the change in FSD due to thermodynamic growth or decay represented by freezing or lateral melting. The fourth term, the mechanical floe size redistribution function, describes the change in FSD due to open water creation or lead opening, ridging, and fragmentation.

The mechanical floe size redistribution function Φ is subject to a strong constraint. By integrating each term in (7) over all floe sizes and recalling (6), we can obtain

$$\int_0^\infty \Phi dl = \nabla \cdot \mathbf{u}. \tag{8}$$

The integral of the third term in (7) represents the change of total area (open water and ice) by thermodynamics which must be zero [*Thorndike et al.*, 1975]. The constraint imposed by (8) allows the model to conserve areas of ice and open water during an event of ice deformation or ice breakup.

The floe size redistribution function may be separated into three terms $\Phi = \Phi_0 + \Phi_r + \Phi_f$, representing the mechanical changes in FSD due to open water creation (Φ_0), ridging (Φ_r), and wave-induced ice fragmentation (Φ_f), respectively. In order to be consistent with the open water creation term in the ITD theory (see (2)), Φ_0 must be given as

$$\Phi_0 = (P^{*-1}\sigma_{ij}\dot{\varepsilon}_{ij} + \dot{\varepsilon}_{kk})\delta(l). \tag{9}$$

Equation (9), together with (2), ensures that the amount of open water created is the same in both ITD and FSD equations.

To derive Φ_r, we assume that, in each grid cell, all floes of different sizes have the same ITD. This is likely true when a large floe is broken into smaller floes by waves. (Observations are needed to test this assumption). This assumption suggests that ridging reduces the area fractions of all floes equally. We also assume that ridging-induced ice thickness redistribution all contributes to the changes in the area fractions of floes or FSD. From these assumptions or simplifications, we can derive

$$\Phi_r = \int_0^\infty \Psi_r dh \cdot g_l = -P^{*-1}\sigma_{ij}\dot{\varepsilon}_{ij} g_l, \tag{10}$$

where the integral of Ψ_r over all ice thicknesses results in $-P^{*-1}\sigma_{ij}\dot{\varepsilon}_{ij}$, when (3) is considered.

The ice fragmentation term Φ_f is also subject to a constraint. Because there is no change in total area when ice is fractured, it must satisfy

$$\int_0^\infty \Phi_f dl = 0. \tag{11}$$

To derive the ice fragmentation term, we consider that area redistribution occurs during ice breakup such that the area of a given floe size category loses some amount to other floe size categories and at the same time gains some amount from other categories. This can be described by

$$\Phi_f = -Q(l)g_l(l) + \int_0^\infty \beta(l', l)Q(l')g_l(l')dl', \tag{12}$$

where $Q(l)$ is the redistribution probability function specifying whether ice fragmentation takes place and what categories are to participate in the breakup processes, and $\beta(l_1, l_2)$ is a redistributor of FSD. Similar to the redistributor of ITD $\gamma(h_1, h_2)$ in (3), the redistributor of FSD $\beta(l_1, l_2)$ specifies how ice is transferred from one floe size category to another by breaking, and $\beta(l_1, l_2)dl_2$ can be taken as the area of ice put into the floe size interval $[l_2, l_2 + dl_2]$ when a unit area of ice of floe size l_1 is used up. To satisfy (11), β is subject to the following constraint:

$$\int_0^\infty \beta(l', l)dl = 1. \tag{13}$$

Once (11) is satisfied, (8) is automatically satisfied, which can be verified by the integral of $\Phi_0 + \Phi_r + \Phi_f$ over all floe sizes.

The redistributor of FSD β is an unknown in the redistribution theory, except that it must satisfy (13) mathematically. However, satellite images and aerial photographs of ice floes of varying sizes [e.g., *Rothrock and Thorndike*, 1984; *Holt and Martin*, 2001; *Steer et al*., 2008; *Toyota et al*., 2006, 2011] indicate that ice fragmentation caused by stochastic ocean surface waves is likely to be a random process such that when a piece of ice is broken, it is likely to become floes of any size smaller than the original floe size. No particular size category is favored against other size categories during the breakup processes. In other words, when an area of a given floe size category is destroyed, the area is redistributed equally to all other categories of smaller size. This leads us to construct a redistributor that allows the area of a given floe size l_1 to be transferred to the area of any floe size l_2 between $c_1 l_1$ and $c_2 l_1$ during breakup such that

$$\beta(l_1, l_2) = \begin{cases} 1/(c_2 l_1 - c_1 l_1), & \text{if } c_1 l_1 \le l_2 \le c_2 l_1 \\ 0, & \text{if } l_2 < c_1 l_1 \text{ or } l_2 > c_2 l_1 \end{cases} \tag{14}$$

where c_1 and c_2 are the lower-end and higher-end floe size redistribution cutoff constants, respectively.

The floe size redistribution cutoff constants satisfy $0 < c_1 < c_2 < 1$ to reflect the fact that, when ice fragmentation occurs, bigger floes are broken into smaller ones. To determine the values of these constants, we rely on the assumption that ice breakup and the ensuing floe size redistribution is a random process that does not favor or exclude any size categories. This assumption requires that when floes of any size are broken, floes of any smaller sizes must be able to form. In other words, in a sea ice model that involves a finite number of floe size categories, the minimum size considered in the model must be able to form. This suggests that $c_1 = l_{\min}/l_{\max}$, where $l_{\min}$ is the center of the smallest size category in the model and $l_{\max}$ is that of the largest size category. Furthermore, for simplicity we allow $c_2 = 1 - c_1$ to ensure that a range of other floe size categories would also benefit from the breakup.

As mentioned above, the redistribution probability function Q in (12) specifies whether ice breaks and, if so, which categories are to participate in the redistribution of FSD. It is another unknown in the redistribution theory. However, the use of the redistribution probability function P for ridging in (4) suggests that Q be given by

$$Q(l) = \max\left[\left(1 - \int_l^\infty g_l(l')dl'/c_b\right), 0\right], \tag{15}$$

where constant c_b is a participation factor that specifies an area fraction of ice to participate in breaking. Here we consider the range of the participation factor generally to be $0^+ \le c_b < 1$, where 0^+ is a positive number approaching zero, say, 10^{-12}. When $c_b = 0^+$, Q becomes zero, and no ice fragmentation occurs. When the value of c_b is greater than 0^+, it allows an area fraction of ice to break and to participate in the redistribution of FSD.

While describing two different physical processes, the formulas for P and Q are similar in form. However, when ridging occurs, P gives a higher probability for thinner ice to transfer to thicker ice. When breakup occurs, on the other hand, Q gives a higher probability for ice of larger sizes to transfer to ice of smaller sizes. In fact, (15) specifies that a c_b area fraction of ice with the largest floe sizes is preferentially fragmented during a breakup event. This preference is based on field observations or model analyses that when waves propagate into ice, larger floes are easier to break because they are subject to larger flexure-induced stresses or strains, while smaller floes are likely to ride with waves with little bending [e.g., *Meylan and*

Table 1. The Lower and Upper Limits, Widths, and Centers, All in m, of the Floe Size Categories Partitioned Following a Gaussian Distribution[a]

Category Number	Lower Limit	Upper Limit	Width	Center
1	−0.1	0.1	0.2	0.0
2	0.1	10.2	10.1	5.2
3	10.2	40.2	30.0	25.2
4	40.2	99.8	59.6	70.0
5	99.8	199.1	99.3	149.5
6	199.1	347.9	148.8	273.5
7	347.9	556.0	208.1	451.9
8	556.0	833.1	277.1	694.5
9	833.1	1189.2	356.1	1011.2
10	1189.2	1633.9	444.7	1411.5
11	1633.9	2176.8	542.9	1905.3
12	2176.8	2827.7	650.9	2502.2

[a]Floe size is described by caliper diameter l.

Squire, 1994; *Squire et al*., 1995]. It is also based on simple reasoning: in a given area under the forcing of waves, winds, and currents, larger floes have higher areal coverage and therefore higher probability to break than smaller floes, assuming all floes have the same ITD.

Thus, the participation factor c_b in the redistribution probability function Q plays a prominent role in determining whether wave-induced ice fragmentation takes place and what area fraction of ice floes of large sizes is allocated to participate in the mechanical floe size redistribution. Needless to say, the value of c_b depends on wave conditions, which in turn depend on wind speed and fetch (the distance of open water over which winds is blowing) [e.g., *Squire et al*., 1995; *Thomson and Rogers*, 2014]. It also depends on sea ice conditions because wave propagation and attenuation under ice are affected by ITD and FSD which also control the flexural strength and hence the bending failure of sea ice in the MIZ [*Wadhams et al*., 1988; *Squire et al*., 1995, 2009; *Kohout and Meylan*, 2008; *Dumont et al*., 2011; *Meylan et al*., 2014]. In other words, the value of c_b is a function of ITD, FSD, waves, and wave-ice interactions. In particular, under certain conditions such as calm winds, small waves, or ice of sufficiently strong flexural strength, the value of c_b would be set to 0^+ to reflect the fact that no ice breakup occurs.

4. Numerical Experiments

In this study, we do not attempt to quantify the relationship between the participation factor c_b and ITD, FSD, waves, and wave-ice interactions. Rather, through a series of simplified numerical experiments, we explore the FSD theory's behavior in mechanical floe size redistribution and resulting FSD in various idealized scenarios of ice fragmentation associated with different values of c_b. This gives a qualitative picture of whether the theory and its numerical implementation are able to create features of ice floes often observed in the MIZ. It would also give us clues about the possible range of c_b values in the real world under varying sea ice and wind and wave forcing conditions. We also explore other properties of the mechanical floe size redistribution in the FSD theory, including model sensitivity to the partition of the floe size categories, to the floe size redistribution cutoff constant c_1, and to ridging and open water creation.

In order to focus on the properties of mechanical floe size redistribution due to wave-induced ice fragmentation, the ice advection (the second) and thermodynamic (third) terms in (7) are ignored. Future work needs to consider advective and thermodynamic contributions. The simplified (7) (without advection and thermodynamics) is then implemented numerically in an idealized zero-dimensional ITD and FSD sea ice model which aims only at the processes of mechanical floe size redistribution described by Φ. In the numerical experiments with the idealized sea ice model, the ITD equation (1) is not actually computed. However, we assume (1) provides the area fraction of open water and ridging term (Ψ) for the integration of the simplified (7). The numerical implementation of (7) requires discretization in the floe size (l) domain to create floe size categories. To examine the model behavior with the partition of floe size categories, (7) is discretized in the l domain following two partitions.

Partition 1 has $M = 12$ floe size categories, partitioned following a Gaussian distribution [see *Hibler*, 1980, Appendix C] to obtain a floe size mesh that varies smoothly in space (Table 1). Here M is the total number of categories used in the model. Using this method, the widths and centers of the floe size categories increase toward the high end of the partition following the Gaussian distribution. The first floe size category has a zero center, $l_1 = 0$, representing the open water category (Table 1). The second floe size category has the smallest nonzero center, $l_2 = l_{\min} = 5.2$ m. The 12th category, or category M, has the largest center, $l_{12} = l_{\max} = 2502.2$ m. Thus, using 12 categories, Partition 1 is able to resolve relatively small floes while including large floes up to ~2.5 km in caliper diameter. As shown in section 3, the centers of the smallest and largest categories (categories 2 and M) are used to determine the redistribution cutoff constant c_1 in (14).

Some observational studies partitioned floe size categories with a uniform width [e.g., *Rothrock and Thorndike*, 1984]. This is followed for Partition 2 which has $M = 28$ floe size categories. With the exception of the first category that is the same as Partition 1 for open water, all the other categories with Partition 2 are specified to have a uniform width of 100 m. As a result, the second floe size category has the smallest center, $l_2 = l_{min} = 50.1$ m, while the 28th category (category M) has the largest center, $l_{28} = l_{max} = 2650.1$ m. This means that the floe size range covered by Partition 2 is close to that covered by Partition 1 whose largest category center is $l_{max} = 2502.2$ m, as shown above. Although Partition 2 has more categories, its l_{min} is almost 10 times larger than the l_{min} in Partition 1, thus having a coarser resolution for small floes and larger redistribution cutoff constant c_1. Both partitions are implemented in the simplified (7) for a series of idealized numerical experiments listed below:

1. To examine the model sensitivity to varying values of participation factor c_b, representing varying magnitudes of ice breakups, the model is integrated with three different values of $c_b = 0.05$, 0.10, and 0.50, which remain unchanged in all ice breakup events (section 5.1).
2. Additional experiments related to c_b are conducted to mimic varying fragmentation scenarios that might occur in the wake of storms, in which the values of c_b decrease in some breakup events because of, for example, weakening winds (section 5.2).
3. To examine the model sensitivity to varying degrees of ridging described in (10), two numerical experiments are conducted. One assumes that in a given MIZ area there is a 10% reduction in ice area due to ridging, and the other 20% (section 5.3).
4. To examine the model sensitivity to varying redistribution cutoff constant c_1, two more numerical experiments are conducted in which c_1 is chosen to be l_3/l_{max} and l_4/l_{max}, respectively (section 5.4).

5. Results

In all the numerical experiments mentioned above, the simplified (7) (without advection and thermodynamics) is integrated over a succession of ice breakup events, with the initial ice floe condition specified to consist of only those within category M with a center of l_{max}. Other initial ice floe conditions are possible, such as those with floes in a number of categories. However, in the simplified numerical experiments, we are focusing on the spring-to-summer breakup of the ice, when the ice cover often starts out as one big plate and breaks into pieces under mechanical forcing. Different ice floe conditions are represented in the evolution of FSD associated with the succession of ice breakups. The ice breakup events are assumed to occur in a typical, fixed MIZ area, which consists of a fraction of open water, with the rest covered by sea ice. Here for simplicity the area fraction of open water is fixed to be a constant of 0.2 for all numerical experiments. This number was chosen based on *Doble and Bidlot* [2013] who use it as a threshold below which pack ice is allowed to break in their wave model simulations. Note, however, that choosing a different area fraction of open water does not fundamentally change the outcome of the experiments.

5.1. Model Behavior With Varying Participation Factors and Partitions of Floe Size Categories

Figure 1 shows changes in FSD after varying numbers of ice breakup events from those experiments that use different values of participation factor c_b. After the first ice breakup (black color in Figure 1), the area fraction of the floes in category M, with a center of l_{max}, is reduced from the initial value of 0.8. The rate of decrease depends on the levels of ice fragmentation represented by different values of c_b used. The area lost in category M is redistributed to other categories of smaller sizes. In the following breakups (colors other than black in Figure 1), the area in category M continues to shrink, redistributed further to other categories. Meanwhile some areas of other categories that also have floes of relatively large sizes, such as categories $M-1$ and $M-2$, are also transferred to those of smaller sizes.

As more breakups occur, the area fraction of category M would be depleted, followed by category $M-1$, category $M-2$, and so on (Figure 1). Eventually, the region would be dominated by those categories of smaller floe sizes. This is illustrated by the case of $c_b = 0.5$ that rapidly redistributes floe size from the high end of FSD to the lower end (Figures 1c and 1f). In fact, the ice field is left with only those floes in category 2, the smallest floes allowed in the model, after $\leq$30 breakups. For smaller levels of fragmentation ($c_b = 0.05$

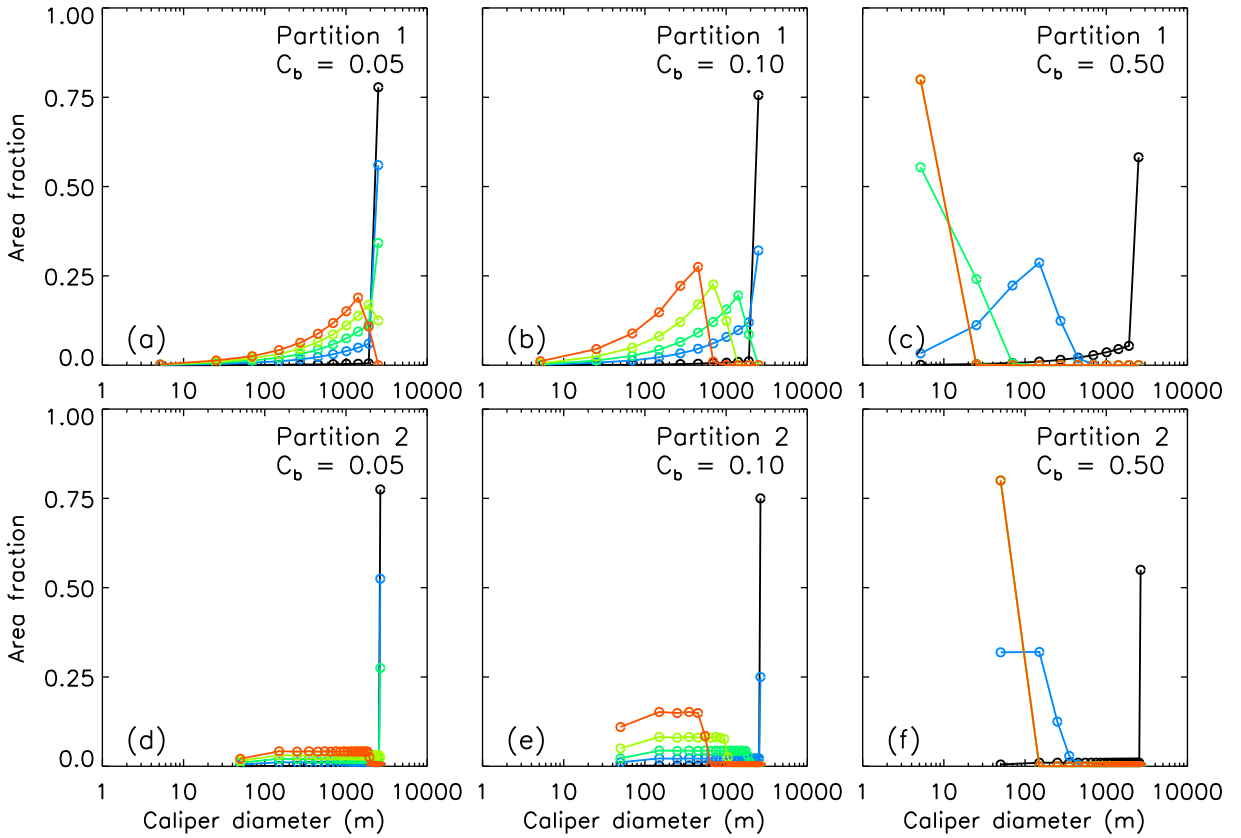

Figure 1. FSD in area fraction, $g_l\Delta l$, after varying numbers of ice breakups, calculated with different floe size category partitions and participation factors of floe size redistribution. Black, blue, green, yellow-green, and red lines and circles represent the first (initial), 10th, 20th, 30th, and 40th ice breakup, respectively. The area fraction of open water category ($l_1 = 0$) is not plotted.

and 0.10), additional breakups are necessary to reach the stage in which floes become small enough to be all included in category 2.

Because the center and width of category 2 with Partition 1 are smaller than those with Partition 2 (section 4), the case of Partition 1 generally needs more breakups to reach that stage in which areas of floes of different sizes are all redistributed into category 2. Using $c_b = 0.5$, for example, it takes ~30 breakups with the case of Partition 1 to reach that stage (Figure 1c, red color overlapping green-yellow color), while it takes ~20 breakups with the case of Partition 2 (Figure 1f, red color overlapping green and green-yellow colors). Once reaching that stage, the case of Partition 1 would have floes with a mean size of ~5 m, while the case of Partition 2 would have floes with a mean size of ~50 m.

Note that in the case of Partition 1, when the area of the largest category, category M, is reduced due to fragmentation, most of the lost area is redistributed to the second largest category, category $M-1$ (Figures 1a–1c). If there is area lost in category $M-1$, most of it is transferred to category $M-2$, and so on. With Partition 2, on the other hand, area lost in a category benefits all categories of smaller sizes almost equally because of the uniform width of the floe size category partition (Figures 1d–1f). This behavior reflects the principle in the FSD theory that when a floe is broken, it disintegrates into floes of any size smaller than the original size without favoring or excluding any particular size. Although appearing different from Partition 2, the mechanical floe size redistribution with Partition 1 does not violate this principle because the widths of its categories increase toward the high end of the partition, with wider categories gaining more area (or more floes) than narrow ones in a breakup event.

Corresponding to Figure 1, Figure 2 shows changes in (reverse) cumulative FSD after varying numbers of ice breakup events. The cumulative FSD (CFSD) is defined as the area distribution of floes with caliper diameter not smaller than l, or CFSD $= \int_l^\infty g_l(l')dl'$. Unlike FSD curves (Figure 1), CFSD curves differ little in appearance

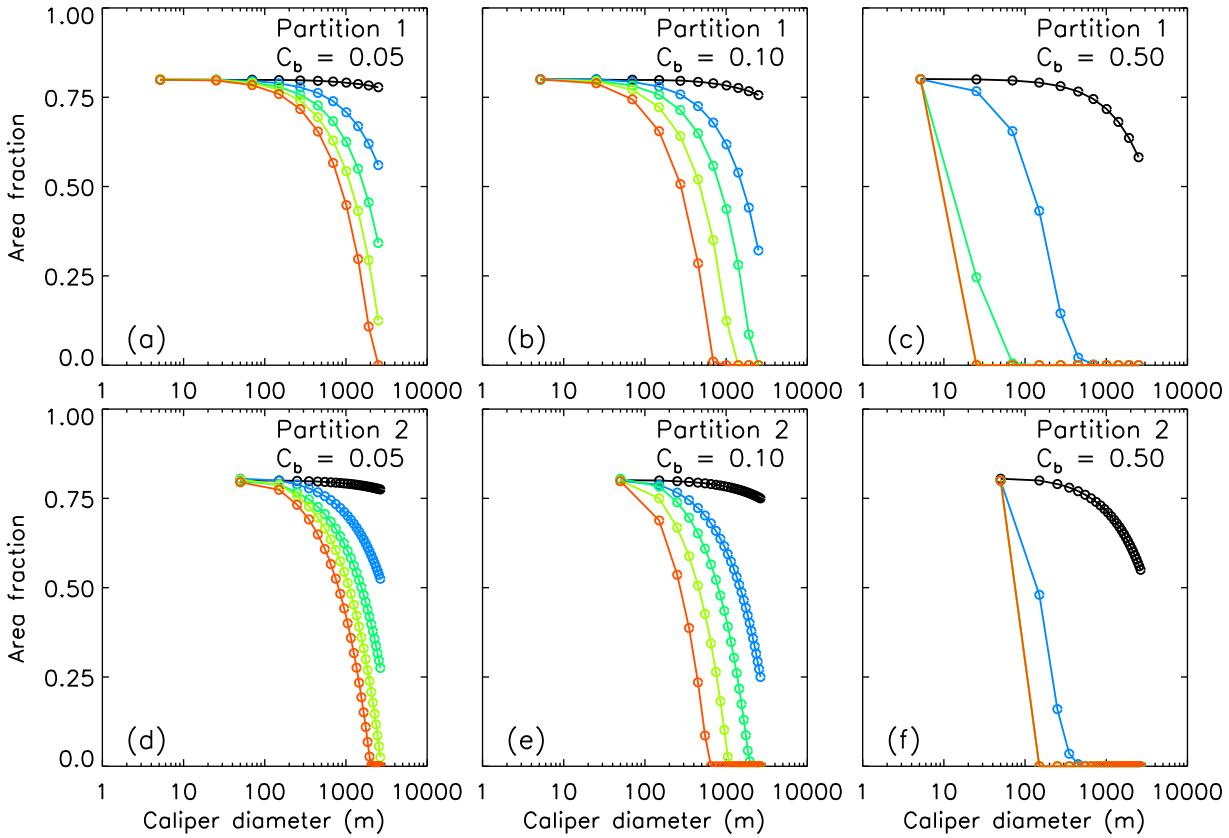

Figure 2. Similar to Figure 1, but with cumulative FSD in area fraction.

between the two sets of partition cases (Figure 2). This is because CFSD is an integration of FSD and therefore does not depend on the widths of the categories, while FSD (in area fraction described by $g_l \Delta l$) does.

Corresponding to Figures 1 and 2, Figure 3 shows changes in CFND or N after varying numbers of ice breakup events. CFND is not a model prognostic variable, but a diagnostic parameter calculated based on FSD, such that $N(l) = \int_l^\infty g_l(l')/(0.66l'^2)dl'$, where $0.66l^2$ is the area of a floe with caliper diameter l following *Rothrock and Thorndike* [1984]. The log-log plots in Figure 3 indicate that the simulated CFND curves mostly obey a power law, whether after an initial breakup (black color), or after varying numbers of breakup events (colors other than black), with either partition cases. This qualitatively agrees with observations [e.g., *Rothrock and Thorndike*, 1984; *Holt and Martin*, 2001; *Toyota et al.*, 2006; *Steer et al.*, 2008]. This is also consistent with the power law behaviors in some random-breaking models [e.g., *Newman*, 2005]. Our power law model results are a direct consequence of the breakup scheme that redistributes large floes to smaller floes.

Except the initial breakup (black color), the CFND curves generally show a steeper descent at or near the high end of the floe size range (Figure 3). This "falloff" from a power law in the model is due to decreasing number, and ultimately disappearance, of floes of large sizes as ice continues to break. Observations of CFND often show a steeper descent also, which is likely due to the same reason or due to limitations of data sampling [*Pickering et al.*, 1995; *Burroughs and Tebbens*, 2001; *Lu et al.*, 2008]. A steeper descent in CFND at the high end of the floe size range may be described by an upper truncated power law [*Pickering et al.*, 1995; *Burroughs and Tebbens*, 2001; *Lu et al.*, 2008]. Away from the falloff zones, the model simulated CFND curves follow a power law with generally straight lines of varying slopes, depending on participation factors and floe size category partitions.

Because the property of a power law is uniquely defined by the absolute value of its exponent α (or slope in log-log space), here we examine α to assess the behavior of the simulated power law. Figure 4 shows changes in slope in a series of consecutive ice breakup events. To avoid the falloff zones as much as possible, the slope in each case is calculated over the first four floe size categories (categories 2–5) if there are at least five categories (categories 2–6) that have floes (not depleted). In other words, as the categories of

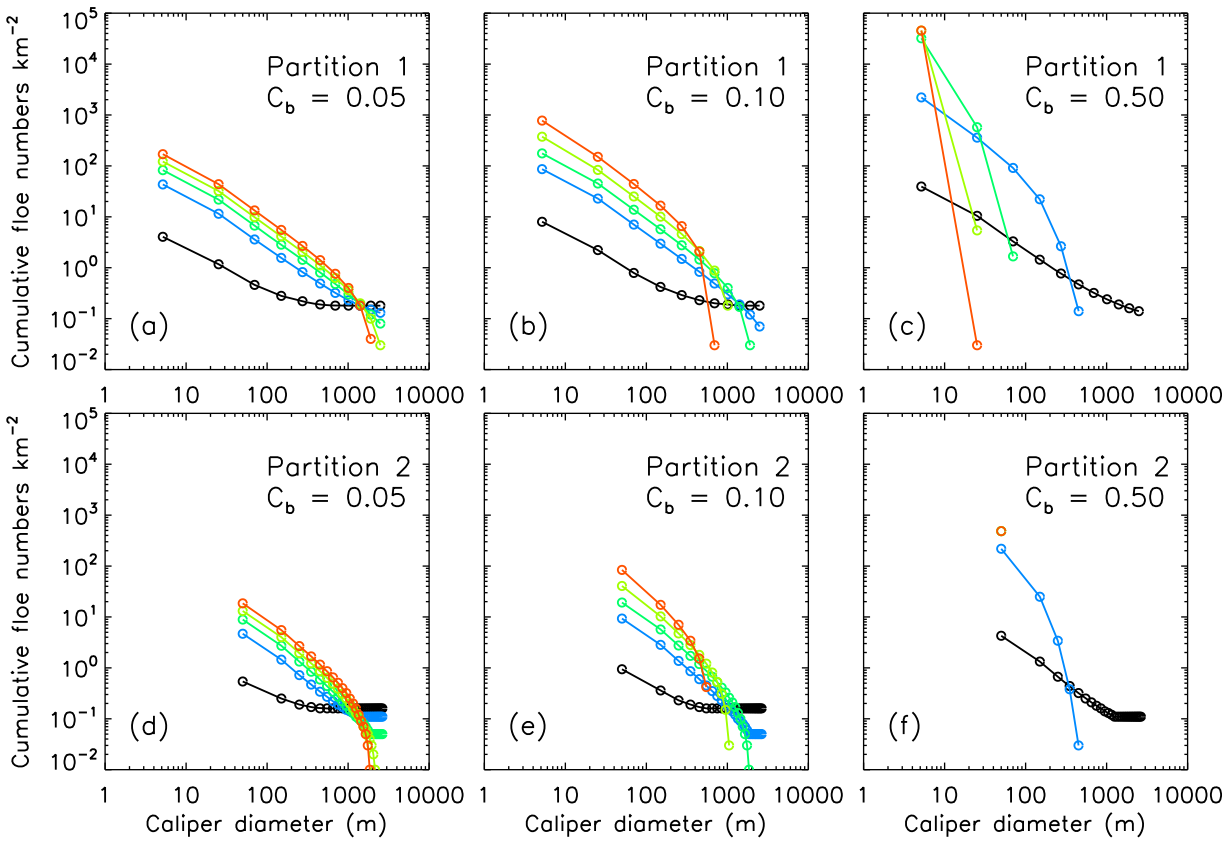

Figure 3. Similar to Figure 1, but with cumulative floe number distribution (CFND, *N*).

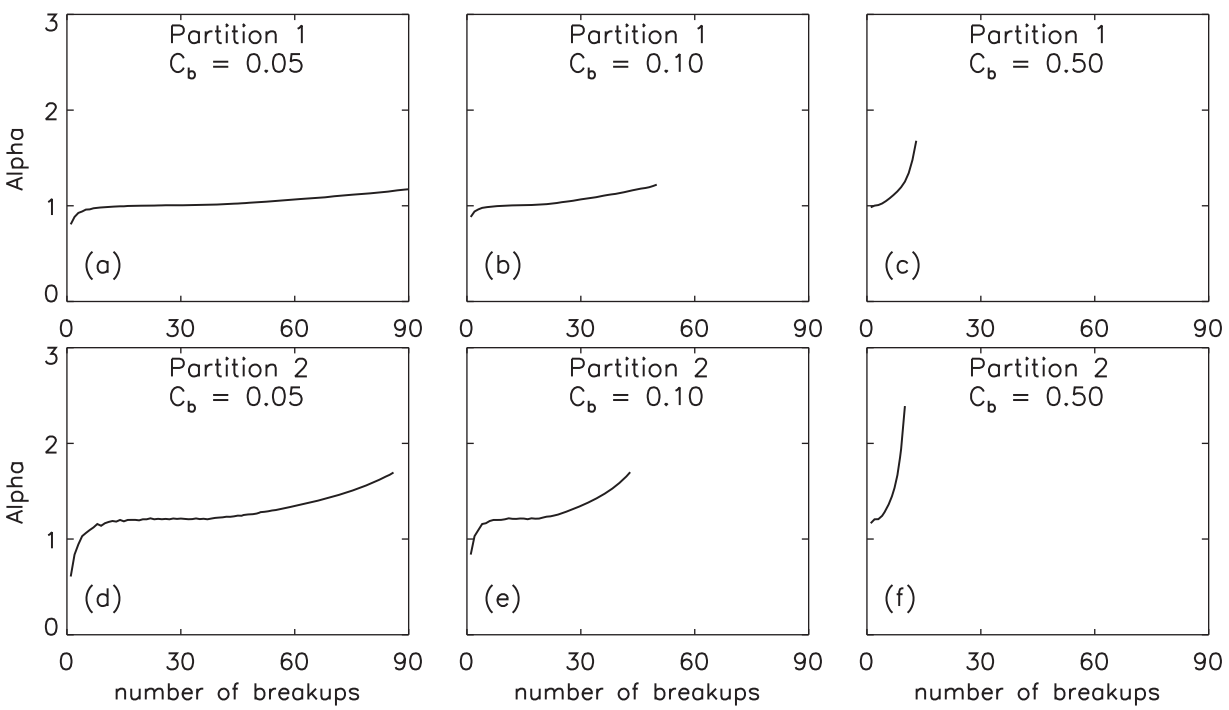

Figure 4. Changes in α in a succession of ice breakups, calculated using different floe size category partitions and participation factors of floe size redistribution.

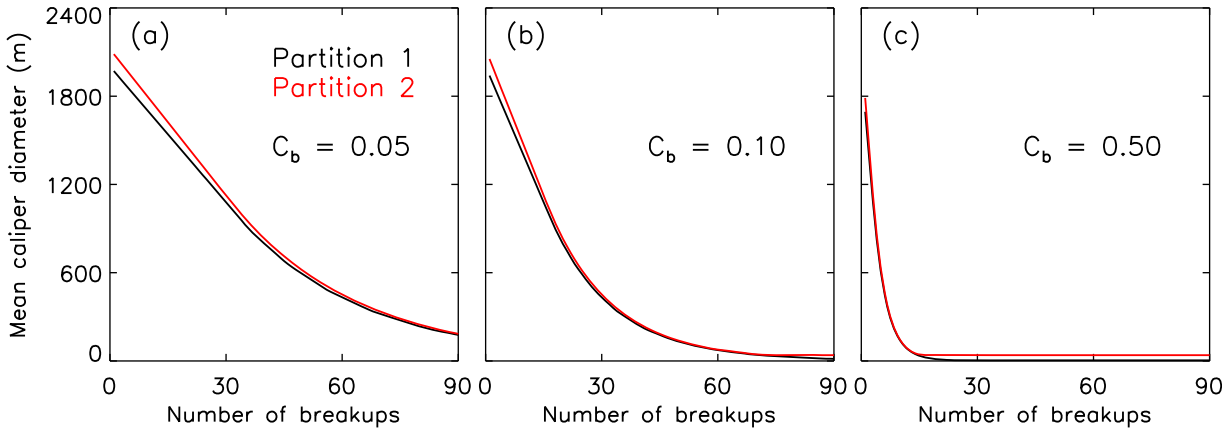

Figure 5. Changes in mean caliper diameter in a succession of ice breakups, calculated using different floe size category partitions, and participation factors of floe size redistribution.

large floes are destroyed one by one in the consecutive breakup events, the slope calculation stops whenever category 6 has no floes. This is why most of slope curves stop short in Figure 4. The calculated slope values generally fall into the range of 1.15–2.90 found by observational studies [*Rothrock and Thorndike*, 1984; *Holt and Martin*, 2001; *Toyota et al*., 2006; *Steer et al*., 2008; *Perovich and Jones*, 2014]. For smaller levels of fragmentation ($c_b = 0.05$ and 0.10), the slope values are below 1.0 in the first few breakup events before climbing above 1.0 (Figures 4a, 4b, 4d, and 4e). For a strong level of breakup ($c_b = 0.50$), the slope values are closer to or above 1.0 right after the first breakup and would increase rapidly afterward, but still remaining below 2.0 or 2.5 within the observational range (Figures 4c and 4f).

Figure 5 shows the evolution of mean floe size or caliper diameter in a series of consecutive ice breakup events. Here mean floe size is defined by $l_m = \int_0^\infty g_l(l) l dl$. Like mean ice thickness $h_m = \int_0^\infty g_h(h) h dh$, mean floe size is an important measure, in addition to FSD, to describe variable floe sizes in a given area. As ice continues to break, l_m decreases, approaching the center of category 2 (l_2) at a varying pace, depending on the level of each breakup event. Ultimately, the ice field is left with the smallest floes within category 2.

An important feature is that the evolution of the mean floe size l_m in either partition is basically the same (two curves almost overlapping in each panel of Figure 5). This indicates that the simulation of floe size redistribution and the resulting FSD and mean floe size do not depend on floe size category partitions, as long as the floe size ranges covered by the partitions are about the same. In fact, if we regroup the FSDs calculated with Partition 1 (Figures 1a–1c) into the categories of Partition 2, the regrouped FSDs would be similar to those calculated with Partition 2 (Figures 1d–1f). This is not true, however, if the floe size ranges in these two partitions differ substantially.

5.2. Model Sensitivity to Varying Breakup Scenarios in the Wake of a Storm

The rapid floe size redistribution with $c_b = 0.50$ is an indication of strong fragmentation (Figures 1–5), which is most likely to occur during storms. Here we conduct three numerical experiments to mimic different breakup scenarios that might occur in the wake of a storm. In these experiments, the initial breakup is all calculated with the value of $c_b = 0.5$, representing a large-scale breakup event at the height of a storm. However, the value should decrease afterward to represent possible changes in the air-ice-ocean conditions in the aftermath of a storm, such as reduced winds or waves and smaller floes that are subject to less bending. In the first experiment of varying c_b (called V1 here), the second through fourth breakups are calculated with c_b values of 0.4, 0.3, and 0.2, respectively, and all the following breakups are calculated with 0.1. In the second experiment (V2), the second through fifth breakups are the same as V1, but all the following breakups are calculated with a value of 0.05. In the third experiment (V3), the second through sixth breakups are the same as V2; after that, no breakups are allowed by setting $c_b = 0^+$. Since the evolution of mean floe size in the FSD theory does not depend on floe size category partitions (Figure 4), only Partition 1 is used in these experiments as well as those presented in following sections.

With varying values of c_b mimicking the different fragmentation scenarios in the wake of a storm, the slope curves from these three cases drift apart after an initial overlap (Figure 6). It is expected that V1 has a largest

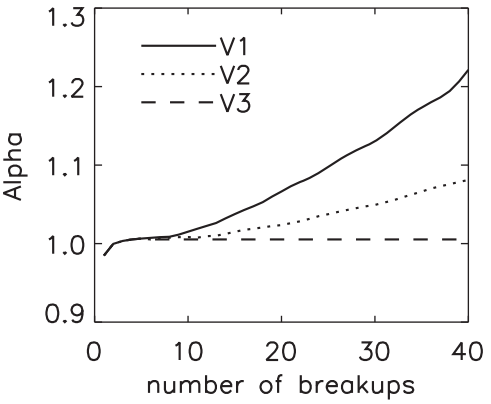

Figure 6. Changes in α in a succession of ice breakups from three numerical experiments using different values of redistribution participation factor, decreasing from the initial value of 0.5, to mimic different scenarios of ice fragmentation in the wake of a storm.

slope than the other two cases because of the largest c_b value (0.1) used for the follow-up breakups after the storm. However, most of the slope values stay above 1.0 and below 1.3. The V3 case is of particular interest. This is because it shows the model is able to prevent ice breakup from happening, as designed in the FSD theory, through the redistribution probability function Q with a zero participation factor. This allows the model to effectively handle the conditions under which no ice fragmentation would take place, such as calm winds and small waves or strong flexural strength of ice.

5.3. Model Sensitivity to Varying Degrees of Ice Ridging

In addition to ice fragmentation, ice deformation-induced ridging may also cause mechanical redistribution of floe size (described in (10)), while open water creation affects the area fraction of the open water category (described in (9)). As described in section 4, two numerical experiments are conducted under the assumption that ice ridging causes a reduction of ice area by 10% and 20%. Note that ridging and open water creation are normally calculated by (1). However, in the simplified sea ice model, (1) is not actually integrated. We just assume that the ridging-induced changes in ice area are provided by (1) in these experiments.

The ridging-induced reduction in ice area means an open water creation by an equal amount. In other words, in these two experiments, the area fraction in the open water category of the FSD is increased by 10% or 20% from the original value of 0.2. The ridging-induced reduction in ice area leads to a reduction in area fraction of all floe size categories (Figure 7). The amount of area reduction in each category is proportional to the area fraction of that category, as described in (10). The case of stronger ridging (20% reduction in ice area) leads to more area reduction across all categories, as expected (Figure 7b). Note that, unlike floe size redistribution due to ice breakup, the ice ridging-induced floe size redistribution assumes no transfer of areas from categories of larger sizes to those of smaller sizes. In other words, no floes of larger sizes break into smaller floes during ridging. Because ridging does not change floe numbers, there is no change in the value of the exponent α.

5.4. Model Sensitivity to Varying Redistribution Cutoff Constants

In the FSD theory, the redistribution cutoff constant c_1 determines the range of floe size redistribution in case of ice fragmentation and is set to $c_1 = l_{min}/l_{max} = l_2/l_{max}$. This ensures that, when an ice floe is broken, categories of smaller sizes all gain floes from the breakup, including the smallest floe size category (Figure 8a). As described in section 4, two more numerical experiments are conducted in which c_1 is chosen to be l_3/l_{max} and

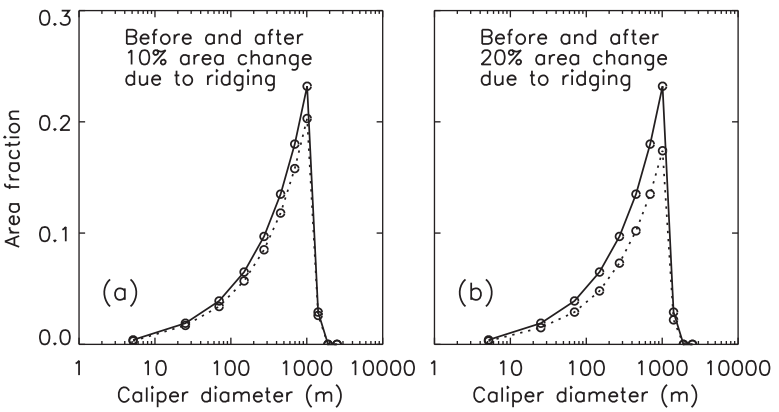

Figure 7. Changes in FSD (dotted line) due to (a) 10% and (b) 20% reductions in ice area induced by ridging.

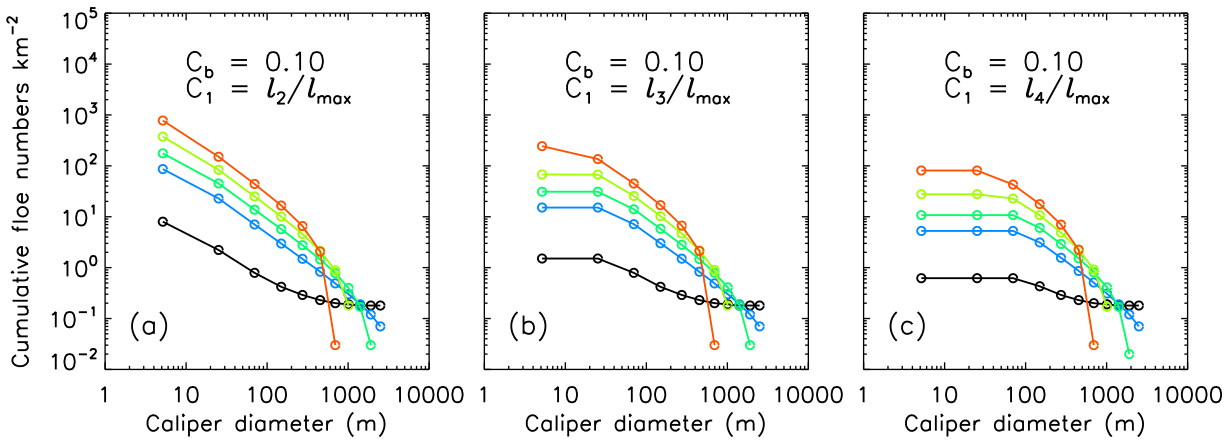

Figure 8. Similar to Figure 3, but with different redistribution cutoff constants c_1 and the same participation factor c_b and Partition 1. For comparison, Figure 8a is a repeat of Figure 3b.

l_4/l_{max}. This means that for the case of $c_1 = l_3/l_{max}$, the second floe size category with the smallest center l_2 may not gain floes when large floes are broken. From the standpoint of physics, this represents a scenario in which large floes are broken into floes of many smaller sizes, but not into floes of the smallest sizes. This is reflected in a "flattening-out" from category 3 to category 2 in the log-log plot of CFND (Figure 8b). For the case of $c_1 = l_4/l_{max}$, both the second and third categories may not gain floes when larger floes are broken. This is reflected in a flattening-out from category 4 to category 2 (Figure 8c). This flattening-out at the lower end of floe size range leads to a local deviation from a power law. In satellite or airborne image analyses of ice floes, similar flattening-out may occur if small floes within a prescribed floe size range are not identified because of limitations of image resolution [*Holt and Martin*, 2001]. In other words, excluding categories at the lower end of the floe size range mimics the resolution limitations in observations, which needs to be avoided whenever possible.

6. Concluding Remarks

Sea ice in the MIZ consists of floes of varying thicknesses and sizes and therefore is better represented by both ITD and FSD. We have developed a FSD theory that is coupled to the ITD theory of *Thorndike et al.* [1975] in order to explicitly simulate the evolution of FSD and ITD jointly. The FSD theory includes a FSD function and an FSD conservation equation in parallel with the *Thorndike et al.* ITD equation. The FSD equation describes changes in FSD caused by ice advection, thermodynamic growth, and lateral melting. It also incorporates changes in FSD caused by mechanical floe size redistribution due to ice ridging induced by ice deformation and fragmentation induced by stochastic ocean surface waves.

The description of mechanical floe size redistribution due to ice ridging and fragmentation is challenging because of our knowledge gaps in various MIZ processes such as ice deformation, wave-ice interactions, properties of ice flexural strength, and patterns of ice breakup. This FSD theory is based on three fundamental assumptions:

1. Ice ridging-induced floe size redistribution is based on the assumption that, at a given area of interest, all floes of different sizes have same ITD, which is likely true when a large floe is broken into smaller floes by waves. This assumption suggests that ridging reduces the area fractions of all floes equally, without area transfer from categories of large floe sizes to those of smaller sizes.
2. Ice fragmentation-induced floe size redistribution is based on the assumption that wave-induced breakup is a random process such that when an ice floe is broken, floes of any smaller sizes have an equal opportunity to form, without being either favored or excluded.
3. Ice fragmentation-induced floe size redistribution is also based on the assumption that floes of larger sizes are easier to break because they are subject to larger flexure-induced stresses and strains; larger

floes also have higher areal coverages and therefore higher probabilities to break than smaller floes. (This is controlled by the participation factor c_b.)

One feature of the FSD theory is that there is only one tunable parameter, the participation factor c_b. The participation factor c_b plays a prominent role in determining whether wave-induced ice breakup occurs and, if so, how many floes of large sizes are to participate in the mechanical floe size redistribution. The value of c_b is linked to wave conditions that depend on wind speed, fetch, and wave-ice interactions. It is also linked to sea ice conditions because ITD and FSD not only affect wave propagation and attenuation under ice but also control the flexural strength and hence the bending failure of sea ice in the MIZ. Thus, c_b is a function of ITD, FSD, waves, and wave-ice interactions. The relationship between c_b and ITD, FSD, waves, and wave-ice interactions needs to be established through observations or model experiments. This study is not aimed to quantify such a relationship. It is aimed to explore the FSD theory's behavior in mechanical floe size redistribution and resulting FSD in various scenarios of ice fragmentation associated with different values of c_b. This gives us ideas qualitatively on whether the theory is able to create features of ice floes often observed in the MIZ. It also give us clues about the possible range of c_b values in the real world under varying sea ice and wind and wave forcing conditions.

To this end, the FSD theory is implemented in a simplified ITD and FSD sea ice model (no advection or thermodynamics) for a series of idealized numerical experiments with different c_b values and floe size category partitions. The model results show that the simulated CFND follows a power law as observed by satellites and airborne surveys. The simulated CFND obeys a power law whether after an initial breakup or after varying number of breakups. Most importantly, the simulated values of the exponent of the power law, with varying scenarios of ice fragmentation represented by different c_b values, are generally in the range of the observations. This indicates that the FSD theory is in a position to realistically simulate power law obeying FSD in the MIZ.

The assumption that wave-induced breakup is a random process without favoring or excluding floes of any smaller sizes plays a key role in obtaining the FSD obeying a power law, as is often the case with random-breaking models. It is found, however, that the simulated CFND would deviate from a power law if categories at the lower end of the floe size range are excluded from participating in redistribution. In other words, if the categories of smallest floes do not gain floes when larger floes are broken, a deviation from a power law is likely to occur locally, with CFND curves flattening out over those categories. A similar deviation may occur in satellite or airborne image analyses of ice floes if small floes within a prescribed floe size range are not identified because of the limitations of image resolution. This suggests the necessity to resolve as many small floes as possible to avoid a deviation from a power law behavior, either in observational analyses or in model simulations.

It is also found that the simulated CFND deviates from a power law by showing a steeper descent at the high end of the floe size range. This is a normal model outcome because of decreasing number, and ultimately disappearance, of floes of large sizes as ice continues to break. The falloff from a power law is often seen in observation-derived CFND, which is likely due to the same reason or due to limitations of data sampling. In some previous studies, the observed falloff behavior at the high end of the floe size range is described by an upper truncated power law. Here the upper truncated power law is replicated in the model.

Another feature of the FSD theory is that mechanical floe size redistribution and the resulting FSD and mean floe size do not depend on how floe size categories are numerically partitioned over a given floe size range. The theory's independence from floe size category partitions over a given floe size range and particularly its creation of the power law obeying FSD seen in nature pave the way to incorporate it into large-scale dynamic thermodynamic sea ice models that are based on the ITD theory of *Thorndike et al.* [1975]. The ability to explicitly simulate multicategory FSD and ITD together may open a door for incorporating additional model physics, such as FSD-dependent ice mechanics and surface exchange of heat, mass, and momentum. The FSD equations also provide a general framework for developing next generation sea ice models to include modeling components to explicitly simulate waves, wave-ice interactions, and wave-induced ice fragmentation in and around the MIZ.

Acknowledgments
We gratefully acknowledge the support of the Office of Naval Research (grant N00014-12-1-0112). We thank two anonymous reviewers for their constructive comments. Model results are available by contacting zhang@apl.washingon.edu.

References

Burroughs, S. M., and S. F. Tebbens (2001), Upper-truncated power laws in nature systems, *Pure Appl. Geophys.*, *158*, 741–757.
Comiso, J. C. (2012), Large decadal decline of the Arctic multilayer ice cover, *J. Clim.*, *25*, 1176–1193.
Doble, M. J., and J.-R. Bidlot (2013), Wavebuoy measurements at the Antarctic sea ice edge compared with an enhanced ECMWF WAM: Progress towards global waves-in-ice modeling, *Ocean Modell.*, *70*, 166–173.

Dumont, D., A. Kohout, and L. Bertino (2011), A wave-based model for the marginal ice zone including a floe breaking parameterization, *J. Geophys. Res.*, *116*, C04001, doi:10.1029/2010JC006682.
Feltham, D. L. (2005), Granular flow in the marginal ice zone, *Philos. Trans. R. Soc. A*, *363*, 1677–1700.
Flato, G. M., and W. D. Hibler III (1995), Ridging and strength in modeling the thickness distribution of Arctic sea ice, *J. Geophys. Res.*, *100*, 18,611–18,626.
Herman, A. (2010), Sea-ice floe-size distribution in the context of spontaneous scaling emergence in stochastic systems, *Phys. Rev. E*, *81*, 066123.
Hibler, W. D., III (1980), Modeling a variable thickness sea ice cover, *Mon. Weather Rev.*, *1*, 1943–1973.
Hibler, W. D., III (2001), Sea ice fracturing on the larger scale, *Eng. Fract. Mech.*, *68*, 2013–2043.
Holt, B., and S. Martin (2001), The effect of a storm on the 1992 summer sea ice cover of the Beaufort, Chukchi, and East Siberian seas, *J. Geophys. Res.*, *106*, 1017–1032.
Kohout, A. L., and M. H. Meylan (2008), An elastic plate model for wave attenuation and ice floe breaking in the marginal ice zone, *J. Geophys. Res.*, *113*, C09016, doi:10.1029/2007JC004434.
Kohout, A.L., M.J.M. Williams, S. Dean, and M.H. Meylan (2014), Storm-induced sea ice breakup and the implications for ice extent, *Nature*, *509*, 604–607.
Langhorne, P. J., V. A. Squire, C. Fox, and T. G. Haskell (1998), Break-up of sea ice by ocean waves, *Cold Reg. Sci. Technol.*, *27*, 438–442.
Lu, P., Z. J. Li, Z. H. Zhang, and X. L. Dong (2008), Aerial observations of floe size distribution in the marginal ice zone of summer Prydz Bay, *J. Geophys. Res.*, *113*, C02011, doi:10.1029/2006JC003965.
Meier, W. N., et al. (2014), Arctic sea ice in transformation: A review of recent observed changes and impacts on biology and human activity, *Rev. Geophys.*, *52*, 185–217, doi:10.1002/2013RG000431.
Meylan, M. H., and V. A. Squire (1994), The response of ice floes to ocean waves, *J. Geophy. Res.*, *99*, 891–900.
Meylan, M. H., L. G. Bennetts, and A. L. Kohout (2014), In situ measurements and analysis of ocean waves in the Antarctic marginal ice zone, *Geophys. Res. Lett.*, *41*, 5046–5051, doi:10.1002/2014GL060809.
Newman, M. E. J. (2005), Power laws, Pareto distributions and Zipf's law, *Contemp. Phys.*, *46*, 323–351.
Perovich, D. K., and K. F. Jones (2014), The seasonal evolution of sea ice floe size distribution, *J. Geophys. Res. Oceans*, *119*, 8767–8777, doi:10.1002/2014JC010136.
Perovich, D. K., B. Light, H. Eicken, K. F. Jones, K. Runciman, and S. V. Nghiem (2007), Increasing solar heating of the Arctic Ocean and adjacent seas, 1979–2005: Attribution and role in the ice-albedo feedback, *Geophys. Res. Lett.*, *34*, L19505, doi:10.1029/2007GL031480.
Perovich, D. K., J. A. Richter-Menge, and K. F. Jones (2008), Sunlight, water, and ice: Extreme Arctic sea ice melt during the summer of 2007, *Geophys. Res. Lett.*, *35*, L11501, doi:10.1029/2008GL034007.
Pickering, G., J. M. Bull, and D. J. Sanderson (1995), Sampling power-law distribution, *Tectonophysics*, *248*, 1–20.
Rothrock, D. A., and A. S. Thorndike (1984), Measuring the sea ice floe size distribution, *J. Geophys. Res.*, *89*, 6477–6486.
Shen, H. H., W. D. Hibler, and M. Leppäranta (1987), The role of floe collisions in sea ice rheology, *J. Geophys. Res.*, *92*, 7085–7096.
Squire, V. A. (2007), Of ocean waves and sea-ice revisited, *Cold Reg. Sci. Technol.*, *49*(2), 110–133.
Squire, V. A., J. P. Dugan, P. Wadhams, P. J. Rottier, and A. K. Liu (1995), Of ocean waves and sea-ice, *Annu. Rev. Fluid Mech.*, *27*, 115–168.
Squire, V. A., G. L. Vaughan, and L. G. Bennetts (2009), Ocean surface wave evolvement in the Arctic Basin, *Geophys. Res. Lett.*, *36*, L22502, doi:10.1029/2009GL040676.
Steele, M. (1992), Sea ice melting and floe geometry in a simple ice-ocean model, *J. Geophys. Res.*, *97*, 17,729–17,738.
Steele, M., J. Zhang, and W. Ermold (2010), Mechanisms of summertime upper Arctic Ocean warming and the effect on sea ice melt, *J. Geophys. Res.*, *115*, C11004, doi:10.1029/2009JC005849.
Steer, A., A. Worby, and P. Heil (2008), Observed changes in sea-ice floe size distribution during early summer in the western Weddell Sea, *Deep Sea Res., Part II*, *55*, 933–942.
Strong, C., and I. G. Rigor (2013), Arctic marginal ice zone trending wider in summer and narrower in winter, *Geophys. Res. Lett.*, *40*, 4864–4868, doi:10.1002/grl.50928.
Thomson, J., and W. E. Rogers (2014), Swell and sea in the emerging Arctic Ocean, *Geophys. Res. Lett.*, *41*, 3136–3140, doi:10.1002/2014GL059983.
Thorndike, A. S., D. A. Rothrock, G. A. Maykut, and R. Colony (1975), The thickness distribution of sea ice, *J. Geophys. Res.*, *80*, 4501–4513.
Toyota, T., S. Takatsuji, and M. Nakayama (2006), Characteristics of sea ice floe size distribution in the seasonal ice zone, *Geophys. Res. Lett.*, *33*, L02616, doi:10.1029/2005GL024556.
Toyota, T., C. Haas, and T. Tamura (2011), Size distribution and shape properties of relatively small sea-ice floes in the Antarctic marginal ice zone in late winter, *Deep Sea Res., Part II*, *58*, 1182–1193, doi:10.1016/j.dsr2.2010.10.034.
Wadhams, P. (1981), Sea-ice topography of the Arctic Ocean in the region 70°W to 25°E, *Philos. Trans. R. Soc. London A*, *302*, 45–85.
Wadhams, P. (1986), The seasonal ice zone, in *The Geophysics of Sea Ice*, edited by N. Untersteiner, pp. 825–991, Plenum, N. Y.
Wadhams, P., V. A. Squire, D. J. Goodman, A. M. Cowan, and S. C. Moore (1988), The attenuation rates of ocean waves in the marginal ice zone, *J. Geophys. Res.*, *93*, 6799–6818.
Williams, T. D., L. G. Bennetts, V. A. Squire, D. Dumont, and L. Bertino (2013a), Wave–ice interactions in the marginal ice zone. Part 1: Theoretical foundations, *Ocean Modell.,* doi:10.1016/j.ocemod.2013.05.010.
Williams, T. D., L. G. Bennetts, V. A. Squire, D. Dumont, and L. Bertino (2013b), Wave–ice interactions in the marginal ice zone. Part 2: numerical implementation and sensitivity studies along 1D transects of the ocean surface, *Ocean Modell.,* doi:10.1016/j.ocemod.2013.05.011.
Zhang, J., and D. A. Rothrock (2001), A thickness and enthalpy distribution sea-ice model, *J. Phys. Oceanogr.*, *31*, 2986–3001.
Zhang, J., and D. A. Rothrock (2003), Modeling global sea ice with a thickness and enthalpy distribution model in generalized curvilinear coordinates, *Mon. Weather Rev.*, *131*(5), 681–697.
Zhang, J., R. W. Lindsay, M. Steele, and A. Schweiger (2008), What drove the dramatic retreat of Arctic sea ice during summer 2007?, *Geophys. Res. Lett.*, *35*, L11505, doi:10.1029/2008GL034005.
Zhang, J., R. Lindsay, A. Schweiger, and I. Rigor (2012), Recent changes in the dynamic properties of declining Arctic sea ice: A model study, *Geophys. Res. Lett.*, *39*, L20503, doi:10.1029/2012GL053545.